Cross-validated Probabilistic Seismic Hazard

WALTER SALAZAR (✉ walter.salazar@catolica.edu.sv)

Universidad Catolica de El Salvador   https://orcid.org/0000-0001-6469-1590

1   Cross-validated probabilistic seismic hazard

2

3   Walter Salazar[1]

4   1. Catholic University of El Salvador

5   Corresponding author: Walter Salazar, e-mail: walter.salazar@catolica.edu.sv

6   Abstract

7   We propose a cross-validated seismic hazard (CVSH) method contrasting time-independent

8   and dependent models via the Poisson and Weibull probability cumulative distributions.

9   Based on the upper-limit spectral accelerations retrieved from the time-dependent models,

10   we infer that in the memoryless Poisson approach, the selected lifetime of buildings is

11   location-dependent rather than a fixed classical value of 50 years for all sites. All models

12   compute the seismic hazard for magnitudes M 5-7.83 by the influence of the interface

13   subduction zone in El Salvador at three locations, the Capital City San Salvador, the Port of

14   Acajutla on the coastline, and Arcatao Town in the North of the country returning average

15   spectral accelerations with less than 10% differences in all cases.

16

19

20

1. Introduction

The time-independent probabilistic seismic hazard assessment is the core of any building design guidelines. After the seminal work of Esteva (1967,1968) and Cornell (1968), and later being Fortran coded by McGuire (1975), this method has been applied extensively around the globe and replicated over and over through several computer codes. On the other hand, Woo's exceptional work (1996) gave us light as an alternative approach to compute free-zone design accelerations and compare with the rigid-zone former method. However, there is a lack of a validation procedure in the results of a memoryless seismic hazard assessment; although, in some cases, this method overestimates peak ground accelerations compared with historical data in California and other parts of the world (Salditch et al., 2020; Stein et al., 2017).

Salazar (2021) studied earthquake interoccurrence times using Weibull and Poisson magnitude probabilities distributions connected with hazard models for the volcanic chain in El Salvador and neighboring Central American countries. Within this article, we augment the work of Salazar (2021) for the interface subduction zone in the region and propose a methodology to cross-validate the classical time-independent seismic hazard schemes via a comparison of time-dependent calculations in a rigid and free-zone fashion.

2. Earthquake Catalog

The Middle America Trench runs parallel to the coast where the Oceanic Cocos Plate submerges underneath the Continental Caribbean Plate at a rate of 7-8 cm/yr. Shallow

43 earthquakes occur in the inclined seismic zone with focal depth less than 60 km, yielding a

44 thrust focal mechanism. We updated the homogenized moment magnitude catalog

45 compiled by Salazar et al (2013), covering the years 1609-2019 employing global

46 earthquake solutions (ISC, 2020; PDE, 2020; CMT Ekström et al., 2012) and special

47 studies that have recalculated origin parameters of large earthquakes (Ambraseys & Adams,

48 1995; Ambraseys, 1995; Guzmán-Speziale, 2005; Leeds, 1974; Molnar & Sykes, 1969;

49 White et al., 2004). The final list contains 1320 events with M 5.0 – 7.83 (Figure 1). The

50 maximum magnitude of 7.83 corresponds to September 7th, 1915, at a depth of 60 km,

51 causing severed damaged in the western part of El Salvador. We propose a seismogenic

52 geometrical delimitation comprising the subduction trench to the south (Lemenkova, 2019),

53 the coastal area to the North, and the depth contours of the subducted slab proposed by

54 Slab's USGS project (Hayes et al., 2012; Salazar et al., 2013). However, epicenters of

55 historical earthquakes (1609-1915) lay outside our delimitation since their locations

56 corresponds to the centers inland of the isoseismal curves rather than being offshore. We

57 consider such location uncertainty in the seismic hazard calculation in Section 3.3. The

58 reverse-slip focal mechanism obeys Hauksson (1990), yielding rakes angles of 45° to 135°

59 and within ±20° of the strike of the trench. The northern limit of the interface subduction

60 zone matches the southern limit of the volcanic chain seismogenic source in Central

61 America (Salazar, 2021).

62 The completeness analysis of the catalog for several magnitude bins relies on Tinti &

63 Mulargia (1985) method; see Table 1 and Figure 2. The catalog and its completeness found

64 the study of the earthquake interoccurrence times in the following section.

65

66   3. Earthquakes Interoccurrence times

67   This section aims to corroborate the time between consecutive earthquakes – the

68   interoccurrence times - that belong to a particular magnitude bin follow a Poisson or

69   Weibull probability distribution. Once we assure that such distributions are adequate to the

70   interface subduction zone seismic activity, we evaluate the seismic hazard employing

71   magnitude likelihood distributions on time-independent and dependent models.

72   The Poisson probability cumulative distribution $F(t)$ is given by:

73    $$F(t) = 1 - e^{-\lambda t} \quad t > 0, \lambda > 0$$ Eq.1

74   where λ is the number of earthquakes per unit time, and t is the interoccurrence time

75   (Anagnos & Kiremidjian, 1988).

76   The cumulative $F(t)$ Weibull distribution with parameters α and β yields (Walpole et al.,

77   2007):

78    $$F(t) = 1 - e^{-\alpha t^{\beta}} \qquad t>0, \; \alpha, \beta > 0$$ Eq. 2

79   We first test the two probability functions depicted in Figure 3 and constants listed in Table

80   2 for several magnitude bins employing the whole earthquake catalog without removing

81   foreshocks and aftershocks. To get the Weibull α and β parameters, we use the algorithm

82   developed by Bean et al. (1981); the Poisson λ constant is a simple count of the number of

83   earthquakes in a magnitude bin. The Root Mean Square RMS is used to represent the error

84   between observed and predicted values. Note that the interoccurrence times are effective

85   after the year of completeness for a specific magnitude bin; otherwise, small and

86   intermediate events might give false information due to the unreported earthquakes before

87   the completeness year. We also use magnitude bins since our objective is to perform

88   seismic hazard calculations.

89   Figure 3 on the left depicts the predicted and observed Weibull probability cumulative

90   distribution vs. interoccurrence times. We also present the linearized Weibull plots on the

91   right to visualize better the goodness to the fit (Abaimov et al., 2008).   Weibull probability

92   distribution yields lower RMS (0.012-0.06) than the Poisson distribution (0.049-0.081) for

93   all magnitudes bins; the linearized plots also reveal the goodness to the Weibull fit; the

94   Poisson distribution does not fit to the seismicity times patters of the subduction interface

95   zone for small magnitudes less than 6, as a logical consequence of incorporating dependent

96   events in the analysis. However, for magnitudes greater than 6, the analysis suggests that

97   the Poisson model can represent the level of seismic activity. We confirm such statement

98   since the α Weibull parameters yields near zero yielding $e^{\alpha} \approx 1$, so Equating the right side

99   of Eq. 1 and 2 would yield similar predicted values.

100

101   Since we assure that Weibull distribution is suitable when all events play in the analysis,

102   we proceed to calculate the conditional probability $f(M)_{t, \Delta t}$ that *gives* the probability that an

103   earthquake within a magnitude bin might happen after an elapsed time Δt once an

104   earthquake has happened at the time t:

105    $$f(M)_{t,\Delta t} = \frac{R(t) - R(t+\Delta t)}{R(t)}$$ Eq. 3

106

107   where $R(t) = 1 - F(t) = e^{-\alpha t^\beta}$. Figure 4 shows the conditional probability for several

108   magnitude bins; in general, the greater the magnitude, the lesser the conditional probability,

109   and the longer the interoccurrence time greater the probability of occurrence. We keep this

110   information to use in the time-dependent seismic hazard assessment of the next section

111   (e.g., Table 2 lists the conditional probabilities for the year 2070).

112

113   We secondly test the Poisson probability function depicted in Figure 5 for several

114   magnitude bins removing from the catalog the foreshocks and aftershocks employing the

115   Gardner & Knopoff (1974) time-distance dynamic window scheme. The RMS yields

116   lower (0.030-0.062) compared with the Weibull previous analysis for all magnitude bins,

117   and Figure 5 shows a good Poisson fit in all cases. It means that removing the dependent

118   events in the catalog effectively converts the seismicity to a Poissonian distribution. Once

119   we have assured that the declustered catalog fits a Poissonian distribution, we proceed to

120   perform the seismic hazard assessment in the next section.

121

122

123

124

125   4. Cross-validated probabilistic seismic hazard (CVSH)

126   This section proposes a cross-validated probabilistic seismic hazard (CVSH) employing the

127   results of the seismicity patterns and probability distributions for the interface subduction

128   zone obtained in the previous section. The CVSH method consists of contrasting the

129   computed spectral ordinates from time-independent and dependent probabilistic schemes in

130   rigid and free-zone fashions to find a suitable building lifetime consistent with the upper-

131   limits of the dependent models. We demonstrate applying the CVSH methodology for three

132   sites in El Salvador that such lifetime is location-dependent rather than a fixed arbitrary

133   value, e.g., 50 years at all sites.

134

135   4.1 Time-independent

136   We present a basic theory of two time-independent models, the classical rigid-zone

137   Cornell-McGuire approach and the free-zone Woo (1993). An in-depth discussion of these

138   methods is elsewhere (e.g., Salazar, 2018).

139   For the rigid zone approach, the mean annual rate $E_{(z)}$ for ground motion z is:

140

141    $$E(z) = v \int_{R=0}^{\alpha} \int_{M_{min}}^{M_{max}} f(M)f(R)P(Z > z|M,R)dRdM \qquad \text{Eq. 4}$$

142   where v is the number of earthquakes per year between the minimum magnitude maximum

143   magnitude M_{max}; $f(M)$ is the probability of a magnitude M and depends on the classical

144   Gutenberg-Richter (G-R) relationship log N = A- BM based on the declustered catalog. $f(R)$

145   is the probability of various earthquake locations at a distance R from the site. $P(Z > z|M,$

146    $R)$ is the probability that a given earthquake of magnitude M and epicentral distance R

147   exceeds the motion level z. The probability of exceedance q of a given ground or spectral

148   motion z for a fixed lifetime of the building L is given by:

149

150 $$q = 1 - e^{-LE(z)}$$ Eq. 5

151

152 An acceleration design level is retrieved usually at 2% and 10% of exceedance.

153 The free-zone approach *f(M)* yields the probability of exceeding *M-ΔM* less the probability

154 of exceedance *M+ΔM* according to a Gaussian distribution that depends on the magnitude

155 error based on the clustered catalog. The equivalent of the number of earthquakes per year *v*

156 and the probability *f(R)* in Eq. 1 is substituted by the Kernel *K* probability function *f(M, R)*

157 that depends on the bandwidth of average distance between earthquake epicenters on

158 several magnitudes.

159

160 For the case of the rigid-zone method, the G-R relationship and magnitude probability *f(M)*

161 is presented in Figure 6a and b, yielding a *B* value of nearly one – typically of tectonic

162 earthquakes worldwide - after the completeness analysis and the declustering process

163 (Gardner & Knopoff, 1974). Figure 7 shows the bandwidth of epicentral distance-

164 magnitude for the subduction interface zone used in the free-zone method.

165

166 4.2 Time-dependent

167 Previous works on time-dependent seismic hazard provided consensus estimates of the

168 magnitude, location, and likelihood of potentially damaging earthquake ruptures in the

169 greater California (Field et al., 2015). They employed physics-based earthquake simulators

170 related to elastic-rebound predictability employing Monte Carlo simulations. We propose a

171 more oriented engineering simplified time-dependent models for rigid and free zones

172 relying on the substitution of the term $f(M)$ on Equation 4 by the conditional

173 probabilities $f(M)t, \Delta t$ yielded from the Weibull distribution analysis and correspondent

174 elapsed times (see Figure 4).

175

176 In the rigid model, the mean rate of occurrence v must be calculated based on the clustered

177 catalog. A key consideration when using time-dependent models for calculating the

178 probability of exceedance in Eq. 5 is to set a lifetime L of one year to consider that a level

179 of motion might be exceeded in the next year after the selected elapse time for a specific

180 earthquake size (Salazar, 2021).

181

182 4.3 Computation of cross-validated probabilistic seismic hazard (CVSH)

183 We computed the seismic hazard at three sites: Capital city San Salvador (89.25°W,

184 13.7°N), Acajutla Port in the coastal area (89.8314°W, 13.5761°N) and the Town of

185 Arcatao at the North of the country (88.7489°W, 14.0936°N). We used the rigid-zone and

186 free-zone methods in a time-independent and dependent fashion. We homogenized the

187 hazard computations establishing the following parameters:

188   a) A flat topography surface integration grid of 0.1° x 0.1 ° in longitude and latitude;

189   b) A minimum and maximum magnitude of 5.0 and 7.83 respectively with a

190   magnitude increment $\Delta M=0.1$; we adopted the maximum magnitude listed in the

191   catalog to avoid bias in the hazard determination due to an increments of such

192   value. Correa-Mora et al. (2009) suggested GPS-derived coupling estimates for the

193   Middle America trench, resolving a weak coupling between the Cocos and the

194   Caribbean plates, so a maximum magnitude of 7.83 seems reasonable in this case.

195   c) The Youngs et al. (1997) ground motion prediction equation (GMPE) developed

196   subduction earthquakes worldwide applicable in the magnitude range M 5-8+

197   setting the interface mechanism and the motion prediction at rock sites class

198   NEHRP A/B; the distance definition is the closest distance to the rupture area;

199   d) A seismogenic fix depth of 30 km;

200   e) A truncation value of 3 standard deviations σ in the GMPE;

201   f) For the free-zone methods: Table 3 shows the magnitude and epicentral

202   uncertainties adopted. Note that the epicentral location uncertainties are larger for

203   historical earthquakes (see Section 2).

204   g) We estimate the peak ground acceleration and 5% damped spectral ordinates for 12

205   structural periods between 0 - 3 s at 2 and 10% probability of exceedance; in the

206   case of the time-independent models, we use a lifetime L of 25, 50, 75, and 100

207   years, and for the dependent models we calculated the accelerations that can stand

208   for the year 2025,2045, 2070, 2095 and 2120 according to the conditional

209   probabilities depicted in Figure 4 for each magnitude bin.

210   h) In the case of the time-dependent models, we assume that we started to build

211   infrastructure in 2020, a year after the last one reported in our earthquake catalog.

212   i) We used and modified the KERFRACT Fortran program by Woo (1996) for the

213   time-independent and dependent free model and developed our HAZARD Fortran

214   code for the rigid zone methods.

215

216   We firstly examine the results for the capital city San Salvador (see location in Figure 1),

217   located about 25 km distant from the coastline. Figure 8a shows that time-independent

218   methods for both rigid and free zone yields practically the same ground and spectral

219   acceleration level for all lifetimes. The longer the lifetime, the more significant the spectral

220   acceleration (see also Table 4). It also confirms that the rigid seismogenic source

221   delimitation and its correspondent level of seismic activity agree with the contributions of

222   gridded sources developed in the free-zone method; it also asserts the quality of the

223   compiled earthquake catalog and its completeness periods. Figure 8b shows the results

224   retrieved from the time-dependent methods; again, the rigid and free-zone yield nearly

225   acceleration levels for all structural periods under consideration; shorter the elapsed times

226   lower the hazard; nevertheless, they are not dependent on the elapsed time themselves after

227   the 2045 year. It is a logical result seeing Figure 4, in which conditional probabilities are

228   above 0.85 for all cases after this year. Although, the analysis reveals an essential feature of

229   the time-dependent methods: the level of spectral acceleration has an upper limit when

230   considering all conditional probabilities in all magnitude bins near or equal to unity (e.g., at

231   the year 2095 or 2120, see Figure 4). On the other hand, classical independent-time models

232   might have no acceleration limitations establishing lifetime and its correspondent

233   probability of exceedance.

234   Let us take as a reference the spectral accelerations giving the chance of all earthquakes to

235   occur to give the conditional probabilities near or equal to 1.0 (e.g. year 2120 in Figure 5

236   and Figure 8b). We can go back to Figure 8a and select a spectrum from the time-

237   independent analysis with a lifetime that better matches the average of time-dependent

238   methods. We suggest in Figure 8c-d that a lifetime of 100 years fits the upper limits of

239   time-dependent methods for both the 2 and 10% probability of exceedance with average

240   spectral differences of 6 and 3% respectively; presumably, such lifetime is the same as the

241   difference between 2120 and 2020 (the start year of construction) in the time-dependent

242   scheme. Note that a classical lifetime of 50 years underestimates by 20% the time-

243   dependent estimations.

244

245   Analyzing the Port of Acajutla at the coastal area (see location in Figure 1), the results

246   imply that time-independent methods - rigid and free-zone- give similar spectral

247   acceleration levels (Figure 9a). Still, time-independent methods are sensitive to the

248   structure's lifetime selection. In this case, the time-dependent accelerations calculated for

249   the year 2095 with conditional probabilities nearly one to all magnitudes (see Fig. 5 and

250   Fig. 9b) pair the spectral motions for 75 years of lifetime with average differences of 7 and

251   3%, respectively, for 2 and 10% exceedance (Fig. 9c-d). Such a lifetime is a different one

252   of San Salvador city - 100 years- and presumably the same 75 years between 2095 and

253   2020. We attribute that such differences of a selected lifetime with San Salvador due to the

254   nearest location of the Acajutla Port to the interface subduction seismogenic source. We

255   build a hypothesis: in the time-independent scheme, a building constructed near an active

256   seismic source might have a shorter period of life, and it must be equal to the time between

257   the start year of construction –in our case 2020 - and the last year to calculate the elapsed

258   times in the time-dependent models. On the other hand, selecting a lifetime at Acajutla Port

259   of 100 years would give spectral accelerations that might have never occurred and increase

260   the building construction cost at the coastal area.

261   To validate our hypothesis above, we also performed a seismic hazard at the Town of

262   Arcatao in the North of El Salvador (see location in Figure 1) 90 km away from the

263   interface subduction zone's northern limit. In general, free-zones methods generate spectral

264   ordinates 10-15% higher than rigid zones methods at longer lifetimes; we attribute such

265   difference due to smooth seismicity patterns created by the Kernel K functions in the null

266   subduction epicenter region from a distant site of the subduction zone with the combination

267   of the epicentral error of 30 km employed in historical shocks analysis (Figure 10a-b, Table

268   3). However, average spectral ordinates from both methods yield similar when comparing

269   the upper limits of time-dependent models and 200 years of lifetime for both 2 and 10%

270   probability of exceedance with average spectral differences of 9 and 7%, respectively (Fig.

271   10a-d). In this case, the accelerations in 2220 on the dependent scheme would also return

272   upper-limit accelerations employing $f(M)t, \Delta t = 1$ as an extension of Fig. 5 to that year. The

273   period of life from a distant site of a seismogenic source must be more extended than a

274   building located inside a seismogenic source. Nevertheless, taking a shorter lifetime (e.g.,

275   the classical 50 years) might underestimate the seismic actions yielding structural damage

276   even far away from the interface subduction seismogenic source if time-independent

277   methods are lonely applied.

278   In practice, structural designers seek seismic coefficients for all possible earthquakes to

279   design a building; then, the time-dependent schemes give maximum spectral accelerations

280   engaging all conditional probabilities near or equal to unity. When using the time-

281   independent methods, one must investigate the lifetime that accords to such time-dependent

282   upper limits; the procedure cross-validates the seismic hazard once the lifetime pairs the

283   time from the starting year of construction and the last year employed to calculate the

284   elapsed times. In general, it seems that the classical lifetime of 50 years obeys more due to

285   a financial interest rather than scientific ones, e.g., such years set as the intermediate-term

286   for which a person can buy and own property, so the risk transfers to the individuals that

287   acquire old buildings (Salazar, 2018).

288

289   4. Conclusions

290   The author has manifested that Weibull probability distributions fit the earthquake

291   interoccurrence times for the interface subduction offshore El Salvador when considering

292   all the catalog events and that the Poisson distribution fits the time between earthquakes

293   when removing dependent events. Consequently, both probabilities distributions

294   successfully give elastic response spectra at three sites in El Salvador, employing time-

295   independent and dependent hazard models in a rigid and free-zone fashion; however, the

296   time-independent calculation produces spectral accelerations that are arbitrary due to the

297   building lifetime speculation. The cross-validated method suggests that the lifetime of

298   structures must be location-dependent rather than an arbitrary value, and if more accuracy

299   is needed, it might be structural period-dependent as well (see Figures 8-10).

300

301   The building lifetime in the time-independent schemes must be selected equal to the time

302   between the start year of construction and the last year to calculate the elapse times

303   agreeing to magnitude conditional probabilities equal or near to unity. It is indeed when the

304   spectral acceleration levels yield the upper-limits in the time-dependent methods. The

305   nearest the building's location to a seismogenic source, the shorter the structure's period of

306   life might be. It is a natural survival process; an individual immersed in a hazardous

307   environment has less life expectancy than another settled in a low threat region.   The

308   selection of a long lifetime might also induce seismic actions that would never happen, and

309   the selection of a short one would underestimate seismic actions even if a building settles

310   away from the seismogenic source. The CVSH methodology might be implemented to risk

311   models if building fragility curves are time-dependent calculated; indeed, the structure's

312   vulnerability is not independent of time as we usually consider using an arbitrarily selected

313   lifetime to calculate the correspondent spectral ordinates in the hazard calculations.

314   The cross-validated seismic hazard (CVSH) naturally implies that the selected lifetime is

315   seismogenic source dependent as well. Then combining several sources simultaneously in a

316   Poisson model setting a fixed lifetime would mislead the resulting spectral accelerations for

317   design. Although the hazard assessment gives spectral motions for the subduction interface

318   zone, we corroborated the lifetime location-dependency due to the volcanic chain zone's

319   influence at three sites under analysis based on Salazar (2021). We confirm that for the

320   nearby sites to the volcanoes centers - San Salvador city and Port of Acajutla -a lifetime of

321   50 and 60 years matches time-independent and dependent models; a lifetime of 75 years is

322   suitable for the Town of Arcatao 55 km away from the volcanic zone axis (Fig. 11a-c).

323   The new seismic code regulations in El Salvador must include a seismic zonation and

324   correspondent lifetimes for each seismogenic source rather than one general zonation that

325   combines all influences of earthquake sources. For example, based on the first instance on

326   the PGA at the three sites evaluated, the coastal area yields 1.3 and 2.5 times more shaking

327   than the central and north parts of the country, respectively. Consequently, the building

328   code may charter three zones and their correspondent spectra due to the interface

329   subduction earthquake's influence with distinctive lifetimes. Our dependent hazard scheme

330   limits the analysis to the maximum magnitude reported in the catalog since conditional

331   probabilities are calculated only for the listed events within magnitude bins. In this case,

332   time-independent methods can incorporate a maximum magnitude (e.g., 0.2 to 0.5 units

333   more than the maximum one listed in the catalogue) after applying the cross-validated

334   procedure explained in this article.

335

341

342   **References**

343   Abaimov, S., D. Turcotte, R. Shcerbakov, J. Rundle, G. Yakovlev, C. Goltz & W. Newman
344   (2008) Earthquakes: recurrence and interoccurrence times. Pure appl. Geophys. DOI
345   10.1007/s00024-008-0331-y.

346   Anagnos, T. & S. Kiremidjian (1984) Stochastic time-predictable model for earthquake
347   occurrences. Bulletin of the Seismological Society of America. Vol. 74, No. 6, pp. 2593-
348   2611.

349   Ambraseys, N. & R. Adams (1995) Large Central American earthquakes 1898-1994.
350   Geophysical Journal International. 127, 665-692.

351   Ambraseys, N. (1995) Magnitudes of Central American earthquakes 1898-1930.
352   Geophysical Journal International. 121, 545-556.

353   Bean, S., M. Heuser & P. Somerville (1981) A Fortran program for estimating parameters
354   in a cumulative distribution function. Scientific report No. 3 AFGL-TR-81-0120, Air Force
355   Geophysical Laboratory, Massachusetts, US. pp. 15.

356

357   Cornell, C. A (1968) Engineering seismic risk analysis, Bull. Seismol. Soc. Am.; 58, p.1583-
358   1606.

359

360   Correa-Mora, F., C. DeMets, D. Alvarado, H. Turner, G. Mattioli, D. Hernandez, C.
361   Pullinger, M. Rodríguez & C. Tenorio (2009) GPS-derived coupling estimates for the Central

362 America subduction zone and volcanic arc faults: El Salvador, Honduras and Nicaragua.
363 Geophys. J. Int. 179,1279-1291.
364

365 Ekström, G., M. Nettles, and A. M. Dziewonski (2012) The global CMT project 2004-
366 2010: Centroid-moment tensors for 13,017 earthquakes, Phys. Earth Planet. Inter., 200-201,
367 1-9, 2012. doi:10.1016/j.pepi.2012.04.002

368 Esteva, L. (1967). Criteria for the construction of spectra for seismic design, presented at
369 Third Panamerican Symposium on Structures, Caracas, Venezuela.
370
371 Esteva, L. (1968). Bases para la formulación de decisiones de diseño sísmico, *Ph.D. Thesis*,
372 Universidad Nacional Auto´noma de México, Mexico City.
373
374 Field, E., Glenn P. Biasi, Peter Bird, Timothy E. Dawson, Karen R. Felzer,
375 David D. Jackson, Kaj M. Johnson, Thomas H. Jordan, Christopher Madden,
376 Andrew J. Michael, Kevin R. Milner, Morgan T. Page, Tom Parsons, Peter M. Powers,
377 Bruce E. Shaw, Wayne R. Thatcher, Ray J. Weldon II, and Yuehua Zeng (2015)
378 Long-Term Time-Dependent Probabilities for the Third Uniform California Earthquake
379 Rupture Forecast (UCERF3) Bulletin of the Seismological Society of America, Vol. 105,
380 No. 2A, pp. 511–543, April 2015, doi: 10.1785/0120140093
381
382 Gardner, J. K. & L. Knopoff (1974) Is the sequence of earthquakes in Southern California,
383 with aftershocks removed, Poissonian? *Bull. Seismol. Soc. Am.* 64, 1363–1367.
384

385 Hauksson, E. (1990) Earthquakes, faulting and stress in the Los Angeles Basin, J. Geophys.
386 Res. 95, 365-394.
387
388 Hayes, G., D. Wald, R. Johnson (2012), A three-dimensional model of global subduction
389 zone geometries, J. Geophys. Res[Online], 2012, B01302,
390 http://earthquake.usgs.gov/research/data/slab/
391
392 Guzmán-Speziale, M., C. Valdés-González, E. Molina, J. Gómez (2005) Seismic activity
393 along the Central American volcanic arc: Is it related to the subducted cocos plate?,
394 Tectonophysics 400, 241-254.
395
396 International   Seismological   Centre   ISC   (2020),   On-line   Bulletin,
397 https://doi.org/10.31905/D808B830
398
399 Lemenkova, P. (2019) Geophysical modelling of the Middle America Trench using GMT.
400 Annals of Valahia Universtiy of Targoviste, Geographical Series, 19(2); 73-94. DOI:
401 10.2478/avutgs-2019-0008.
402

Leeds, D. (1974) Catalog of Nicaraguan earthquakes. Bull. Seismol. Soc. Am. 64 (1974) 1135-1158.

McGuire, R. K. (1975) FORTRAN computer program for seismic risk analysis, US Geological Survey; Open-File Report, p. 76-67.

Molnar, P, & L. Sykes (1969), Tectonics of the Caribbean and middle America regions from focal mechanism and seismicity, Geological Society of America Bulletin 80, 1639-1684.

Preliminary Determination of Epicenters PDE (2020) Bulletin, https://earthquake.usgs.gov/data/pde.php

Salazar, W., L. Brown & W. Hernández, J. Guerra (2013) An Earthquake Catalogue for El Salvador and Neighboring Central American Countries (1528-2009) and its Implication in the Seismic Hazard. *Journal of Civil Engineering and Architecture,* ISSN 1934-7359, USA, Aug., Volume 7, No. 8 (Serial No. 69), pp. 1018-1045.

Salazar, W. (2018) Principles of Probabilistic Seismic Hazard Assessment (PSHA) and Site Effects Evaluation and its application for the Volcanic Environment in El Salvador. Book Chapter "Earthquakes - Forecast, Prognosis and Earthquake Resistant Construction," Chapter 8, pp. 119-146. *InTech Open Science London* ISBN 978-1-78923-949-2. DOI: 10.5772/intechopen.75845.

Salazar, W. (2021) Earthquake interoccurrence times and seismic hazard assessment for upper-crustal volcanic chain earthquakes in El Salvador, are they Poissonian distributed? *Natural Hazards*, https://doi.org/10.1007/s11069-021-04640-w.

Salditch, L., M. M. Gallahue, M. C. Lucas, J. S. Neely, S. E. Hough, and S. Stein (2020). California Historical Intensity Mapping Project (CHIMP): A Consistently Reinterpreted Dataset of Seismic Intensities for the Past 162 Yr and Implications for Seismic Hazard Maps, Seismol. Res. Lett. XX, 1–20, doi: 10.1785/0220200065.

Stein, S., Brooks, E., Spencer, B., Vanneste, K., Camelbeek, T., Vleminckx, B. (2017). Assessing how well earthquake hazard maps work: Insights from weather and baseball. Earth Magazine.

Tinti, S. & F. Mulargia (1985) Completeness analysis of a seismic catalogue. *Ann. Geofis*, 3, 407-414.

441   Walpole, R., R. Myers, S. Myers & K. Ye (2007) Probability & Statistics. Prentice-Hall,
442   Eight editions, pp. 816.

443

444   White, R., J. Ligorría, I. Cifuentes (2004), Seismic history of the middle America
445   subduction zone along El Salvador, Guatemala and Chiapas, Mexico: 1526-2000,
446   Geological Society of America Papers 375 (2004) 379-396.
447
448
449   Youngs, R., S. Chiou, W. Silva & J. Humprey (1997) Strong ground motion attenuation
450   relationships for subduction earthquakes. Seismological Research Letters, 68, 58-73.
451
452   Woo, G. (1996). Kernel estimation methods for seismic hazard area source modeling, *Bull.*
453   *Seismol. Soc. Am.* 86, no. 2, 353-362.
454

Figures
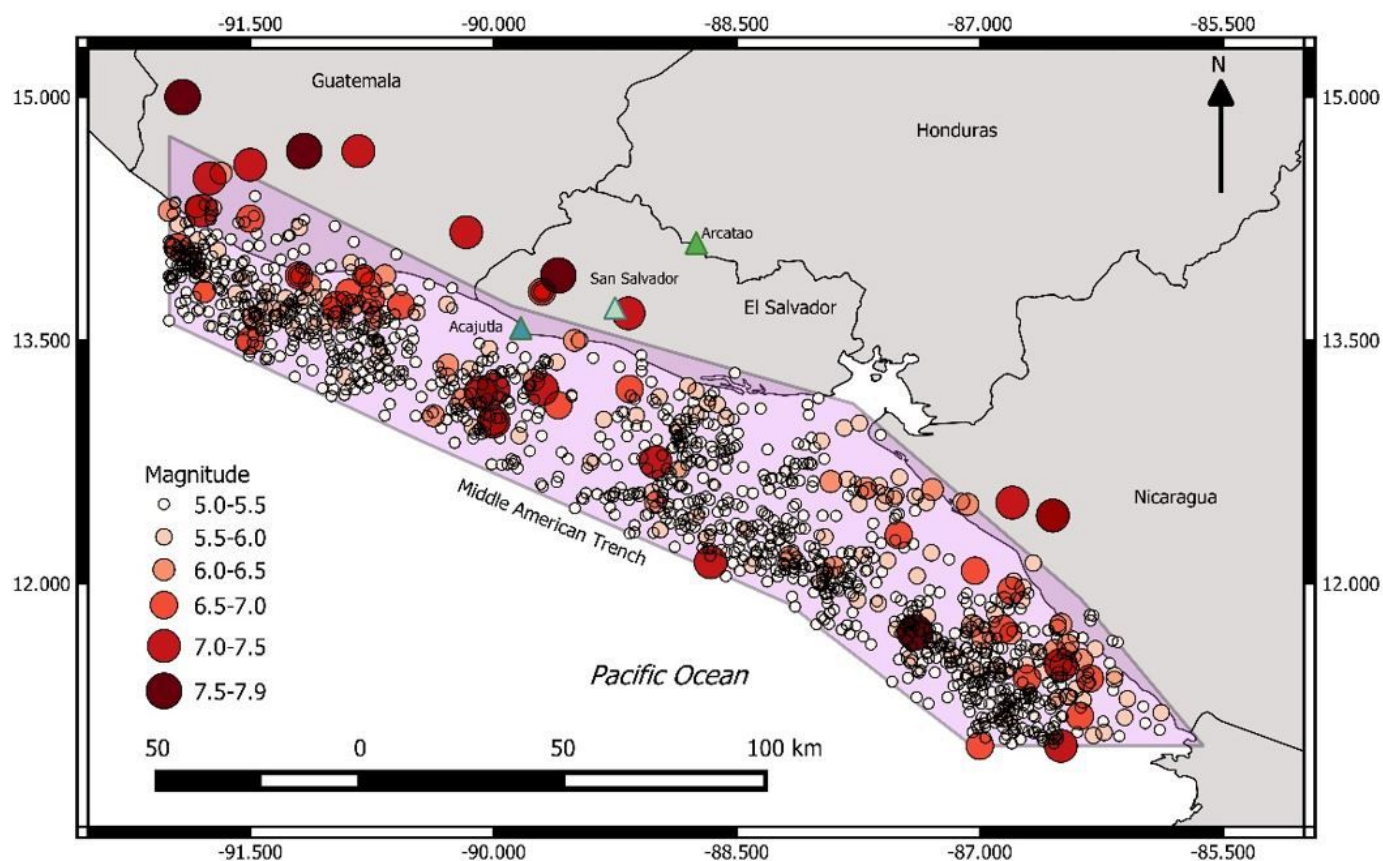
Figure 1

Earthquake epicenters (circles) and geometrical delimitation for interface subduction zone comprising events with moment magnitude 5.0 ≥M≥ 7.83. Triangles denote the location for three sites (Arcatao, San Salvador, and Acajutla), for which we compute the seismic hazard assessment employing time-independent and dependent models. Note: The designations employed and the presentation of the material on this map do not imply the expression of any opinion whatsoever on the part of Research Square concerning the legal status of any country, territory, city or area or of its authorities, or concerning the delimitation of its frontiers or boundaries. This map has been provided by the authors.
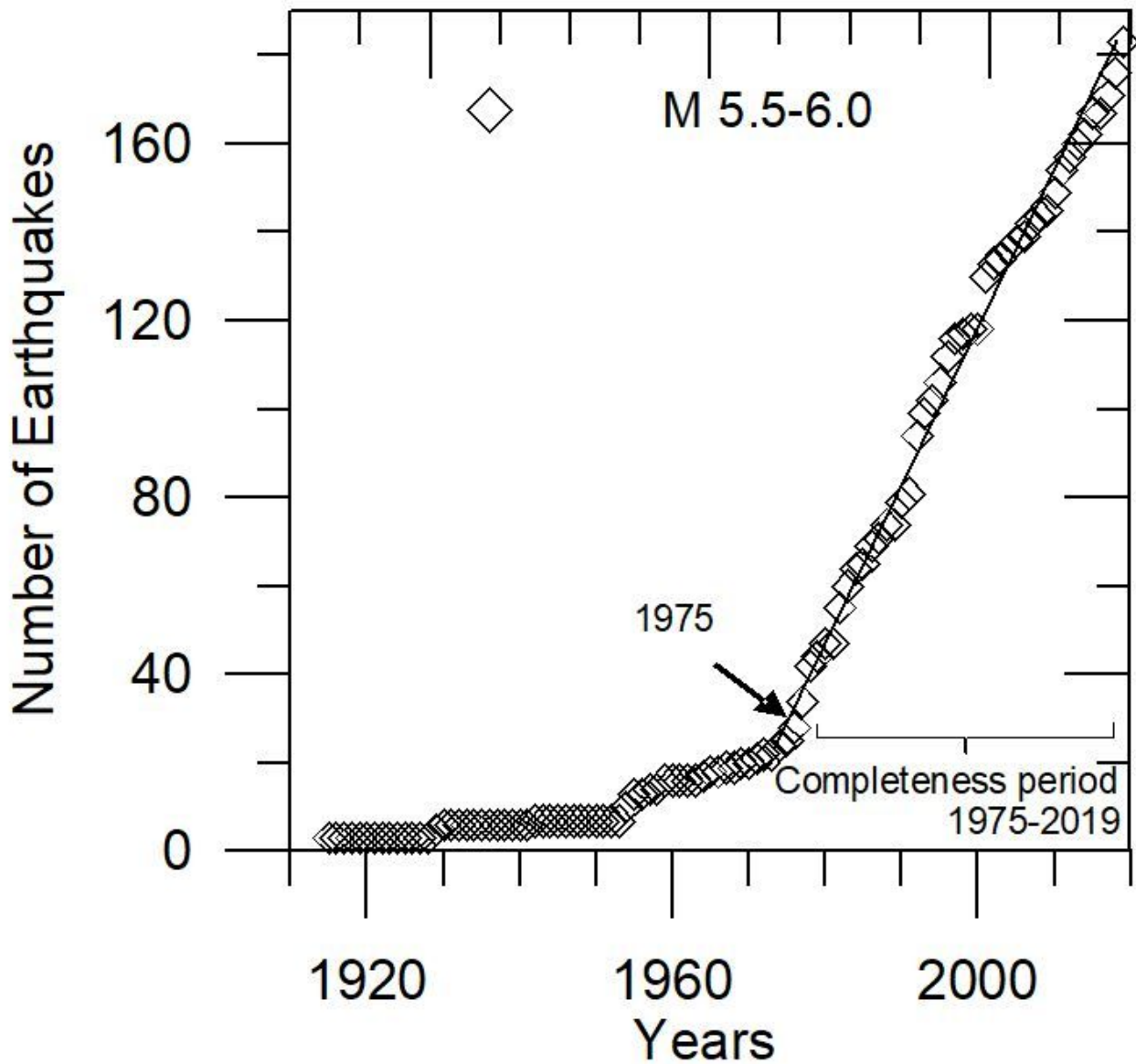
Figure 2

Completeness period for the interface subduction earthquakes within a magnitude bin M 5.5 − 6 employing the clustered catalog. The catalog is complete back to 1975 because the cumulative annual number of earthquakes for this magnitude range is approximately linear back to that date (Tinti & Mulargia, 1985). See the completeness periods for all magnitude bins in Table 1.
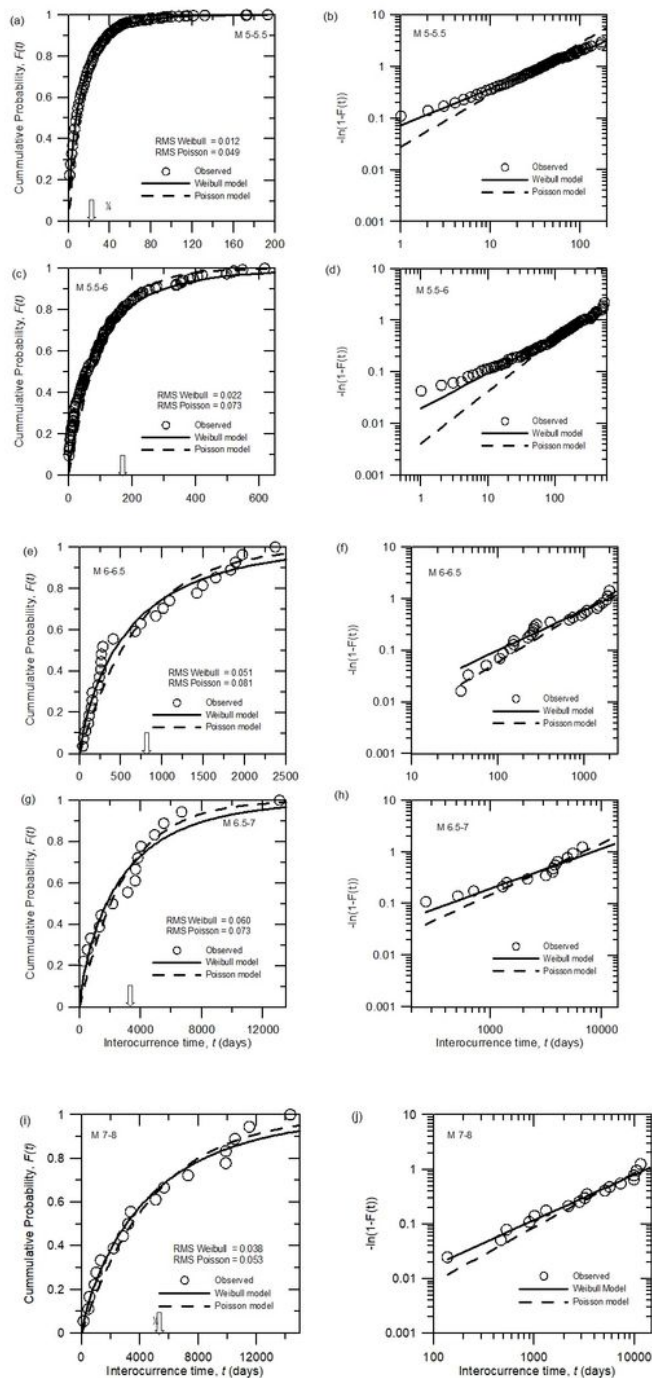
Figure 3

Interoccurrence times vs. cumulative probabilities for several magnitude bins. (a) M 5-5.5 (c) M 5.5-6 (e) M 6-6.5 (g) M 6.5-7 (i) M 7-8. We compare the observed and the estimated cumulative probability distributions employing the Weibull and Poisson models based on the clustered catalog. The arrow depicts Weibull's mean. The right side (b,d,f,h,j) depicts the linearized Weibull plots.
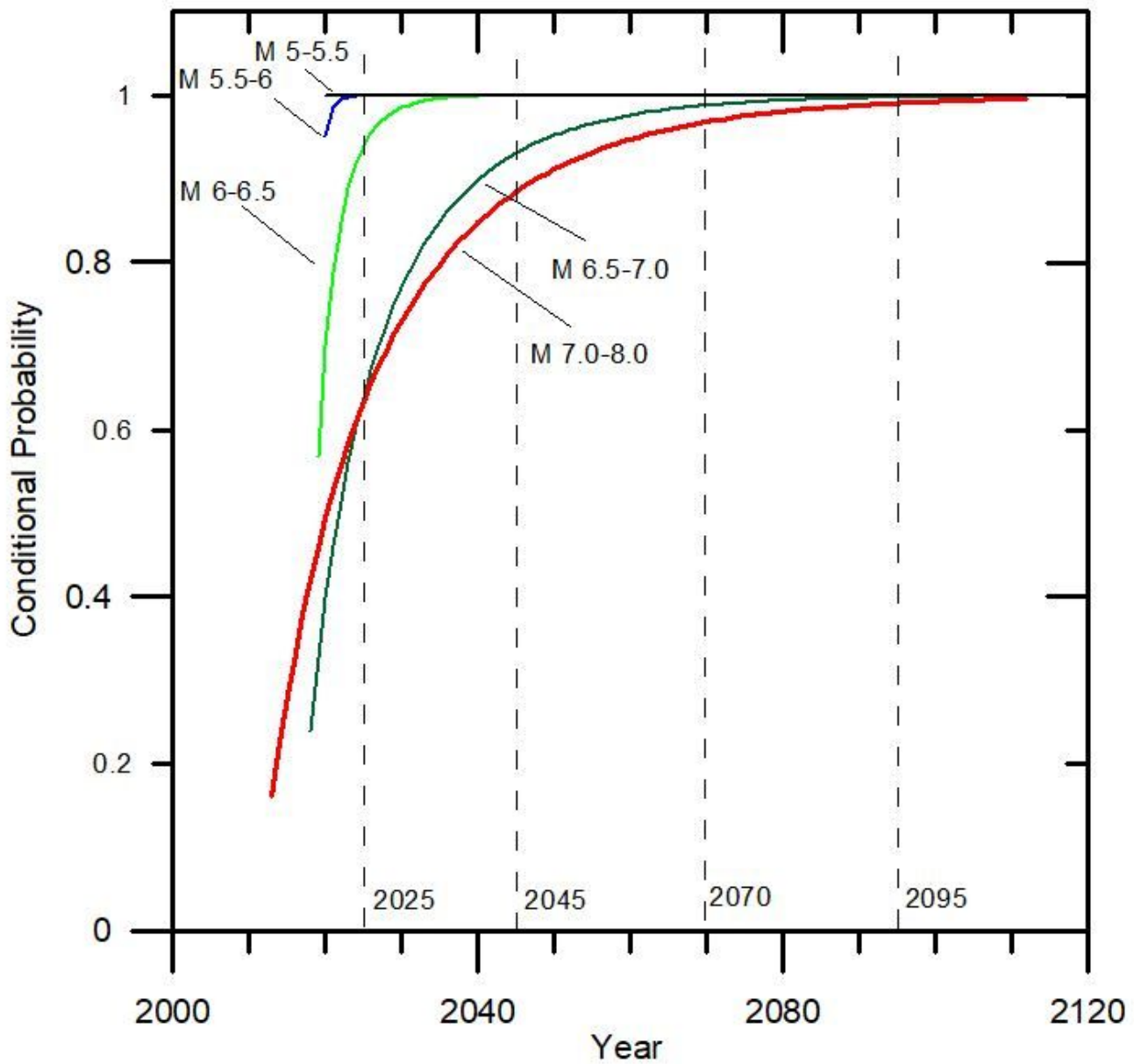
Figure 4

Weibull Conditional Probabilities (Eq. 3) from 1 to 100 years elapsed times. We used each magnitude bin's probabilities in 2025, 2045, 2070, 2095, and 2120 to compute the time-dependent seismic hazard in Figure 8-10.
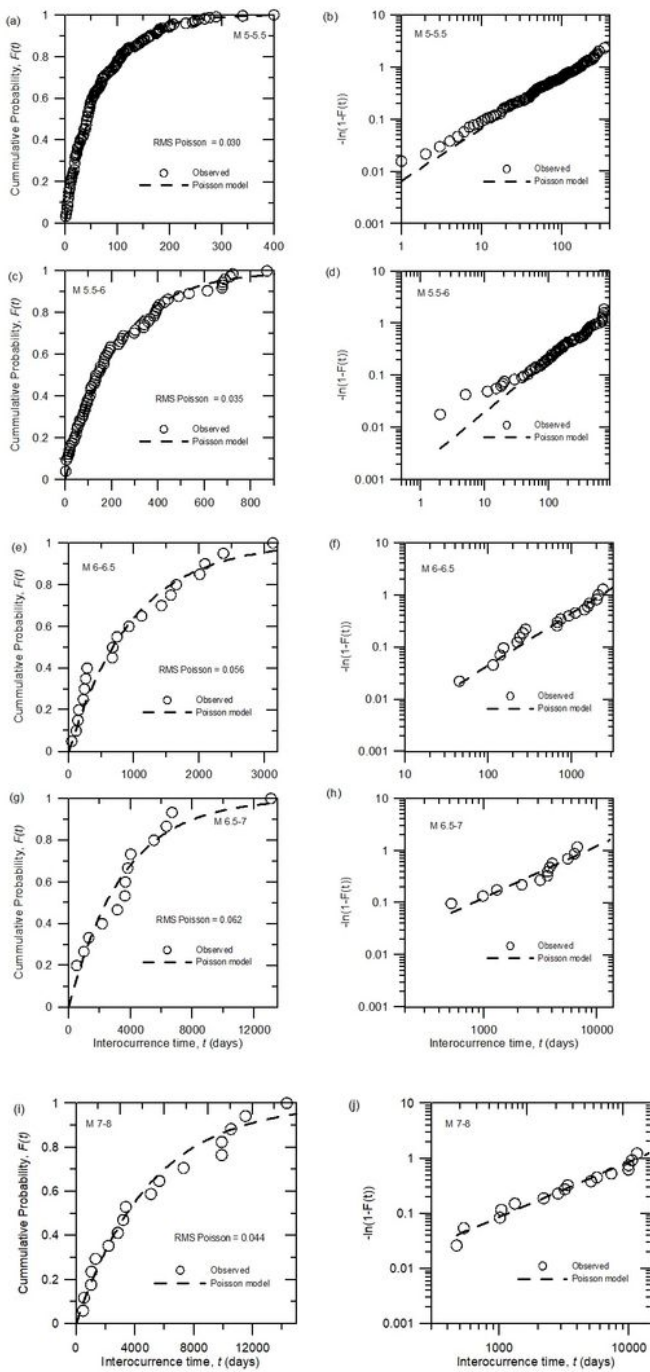
Figure 5

Interoccurrence times vs. cumulative probabilities for several magnitude bins. (a) M 5-5.5 (c) M 5.5-6 (e) M 6-6.5 (g) M 6.5-7 (i) M 7-8. We compare the observed and the estimated cumulative probability distributions employing the Poisson model based on the declustered catalog. The right side (b,d,f,h,j) depicts the linearized Weibull plots.
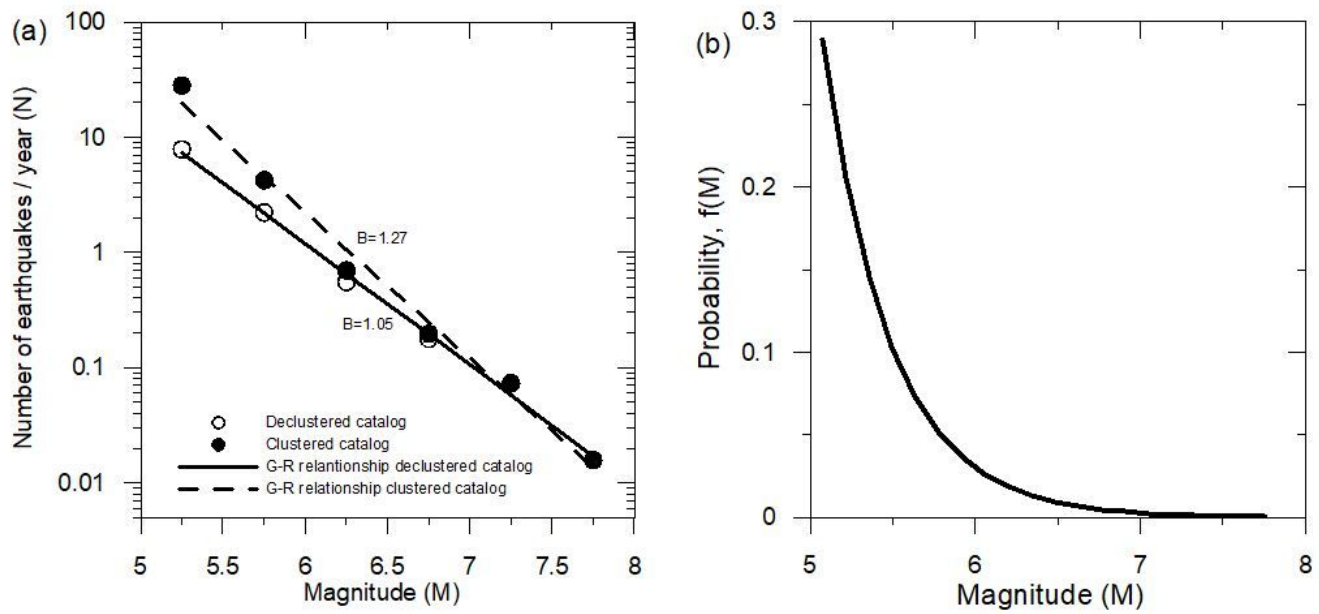
Figure 6

(a) The observed number of earthquakes per year N above a specific magnitude M. The G-R yields log N= 6.40-1.05M, σ=±0.07 and log N = 7.92-1.27M, σ=±0.14 for the desclustered and clustered catalogs (b) Magnitude probability function f(M) for the declustered catalog used in the classical time-independent Poisson scheme.
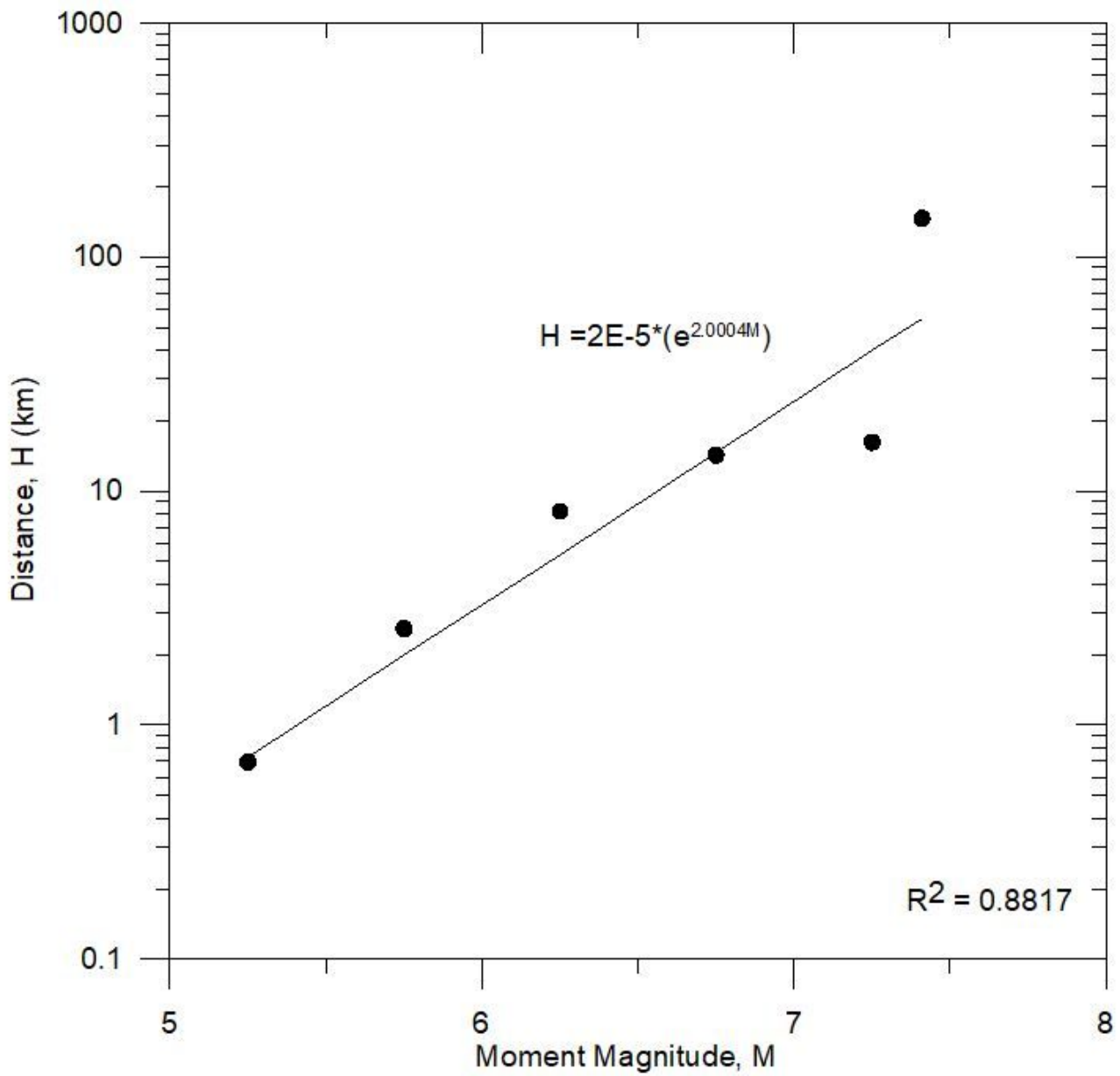
Figure 7

Epicentral average distances in the interface subduction zone for several magnitude bins used in the free-zone methods. R2 is the coefficient of determination.
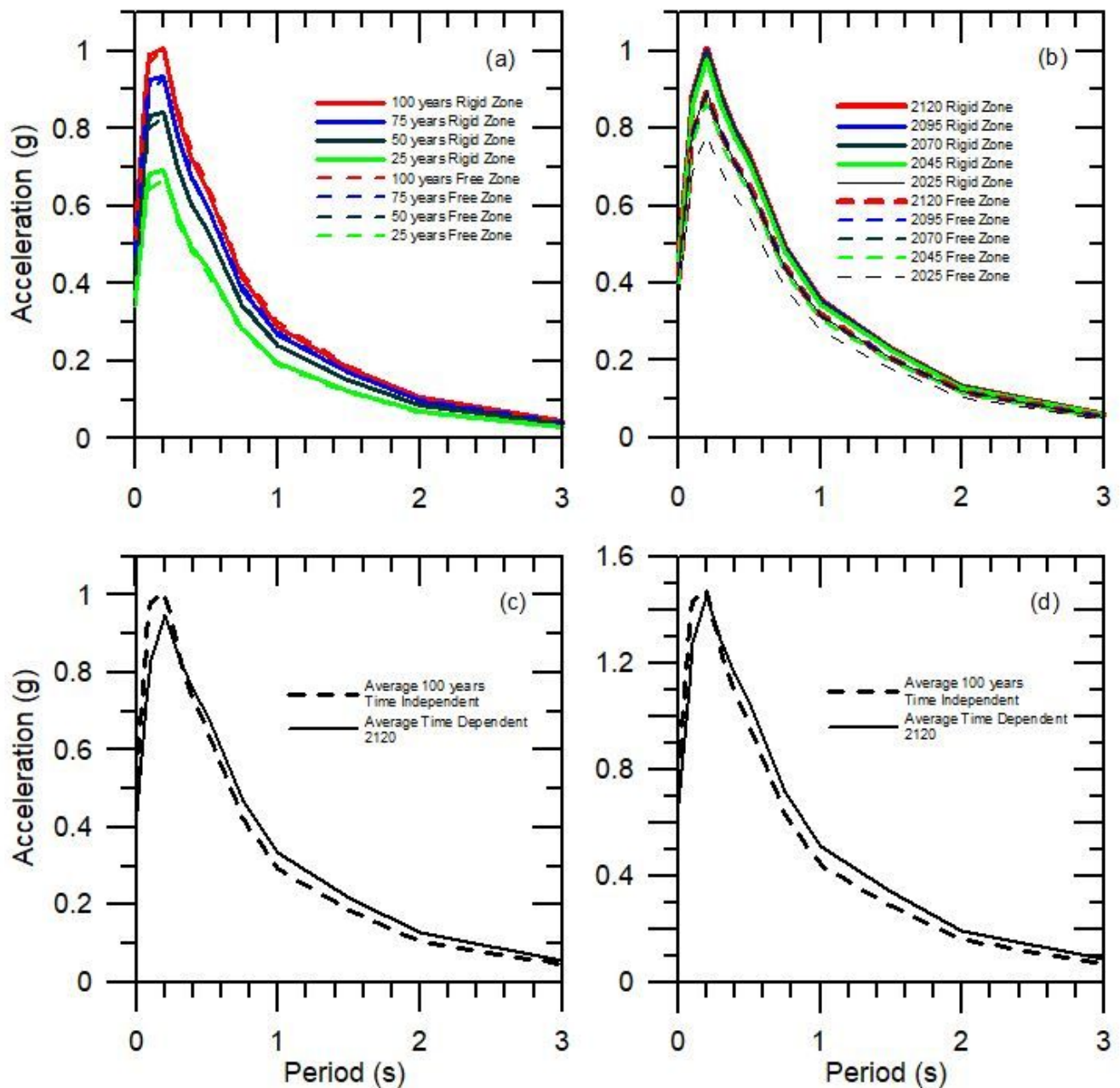
Figure 8

Elastic response spectra for 10% probability of exceedance (a,b,c) employing 5% of critical damping at the capital city San Salvador (89.25°W, 13.7°N; Figure 1). a) Time-independent (TI) models for lifetimes of 25, 50, 75, and 100 years; b) Time-dependent (TD) models for the years 2045, 2070, 2095, and 2120. We used the magnitude conditional probabilities depicted in Figure 5 for such years; c) Comparison of average spectra for TI and TD models; d) Comparison of average spectra for TI and TD models for 2% probability of exceedance.
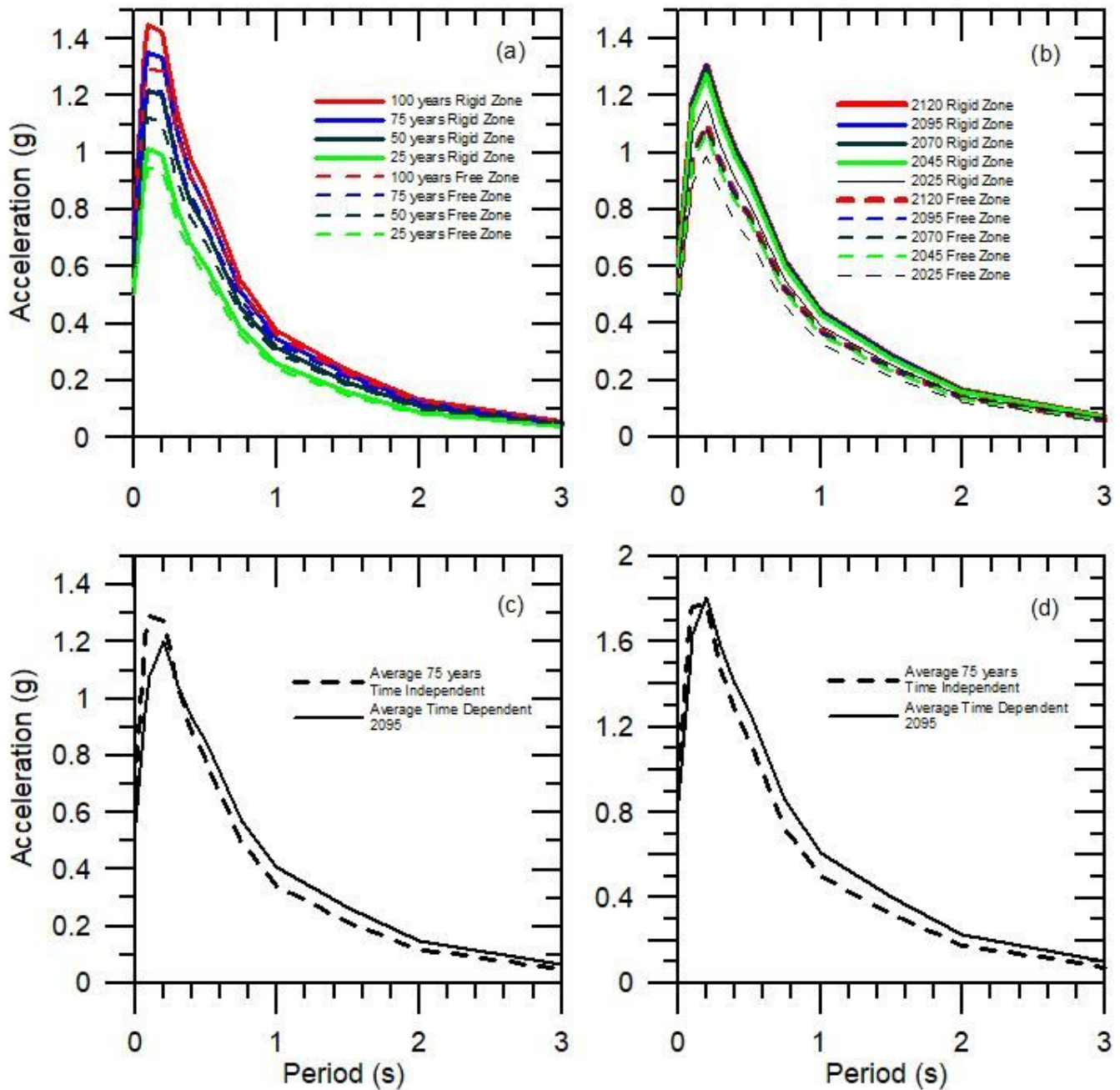
Figure 9

Elastic response spectra for 10% probability of exceedance (a,b,c) employing 5% of critical damping at the Port of Acajutla (89.8314°W, 13.5761°N; Figure 1). a) Time-independent (TI) models for lifetimes of 25, 50, 75, and 100 years; b) Time-dependent (TD) models for the years 2045, 2070, 2095, and 2120. We used the magnitude conditional probabilities depicted in Figure 5 for such years; c) Comparison of average spectra for TI and TD models; d) Comparison of average spectra for TI and TD models for 2% probability of exceedance.
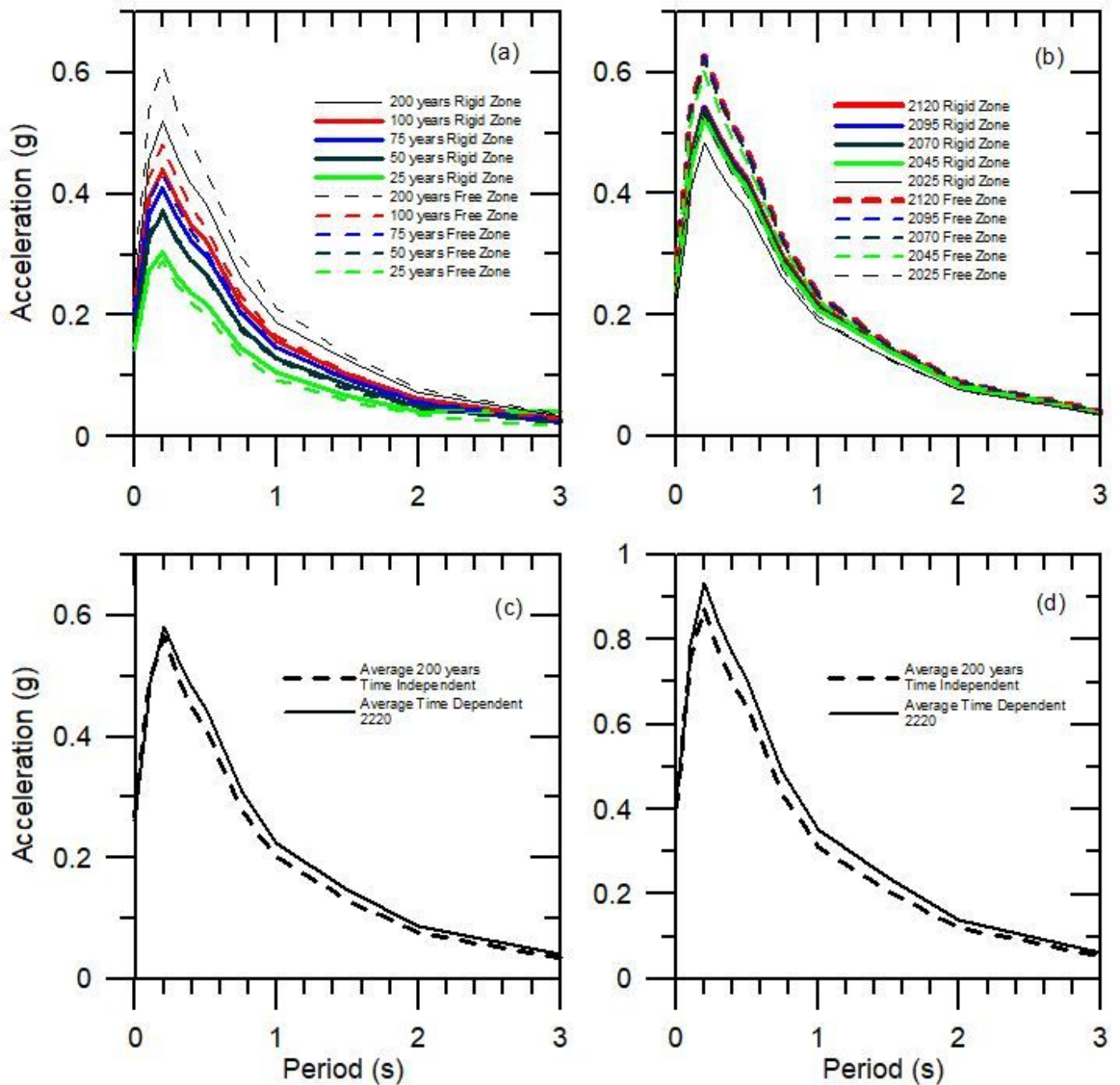
Figure 10

Elastic response spectra for 10% probability of exceedance (a,b,c) employing 5% of critical damping at the Town of Arcatao (88.7489°W, 14.0936°N; Figure 1). a) Time-independent (TI) models for lifetimes of 25, 50, 75, and 100 years; b) Time-dependent (TD) models for the years 2045, 2070, 2095, and 2120. We used the magnitude conditional probabilities depicted in Figure 5 for such years; c) Comparison of average spectra for TI and TD models; d) Comparison of average spectra for TI and TD models for 2% probability of exceedance.
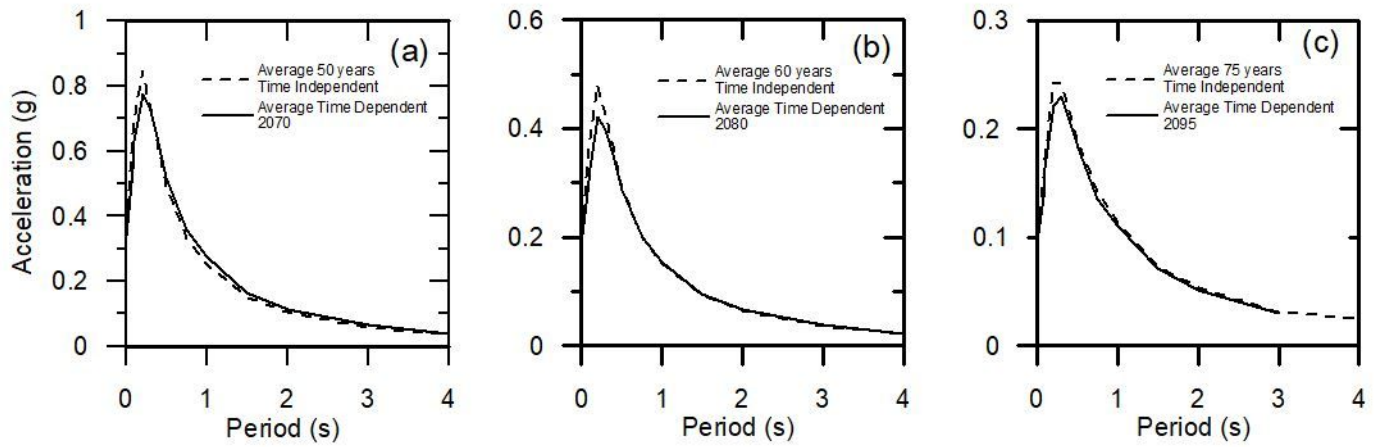
Figure 11

Comparison of average elastic response spectra for time-independent and dependent models due to the volcanic chain's influence (Salazar, 2021); setting 5% of critical damping and 10% probability of exceedance. (a) San Salvador City, (b) Port of Acajutla, and (c) Town of Arcatao (see locations in Fig. 1).